Ca^{2+} Sparks in Embryonic Mouse Skeletal Muscle Selectively Deficient in Dihydropyridine Receptor α_{1S} or β_{1a} Subunits

Matthew W. Conklin,* Patricia Powers,† Ronald G. Gregg,‡ and Roberto Coronado*
*Department of Physiology, University of Wisconsin Medical School, and †Biotechnology Center, University of Wisconsin, Madison, Wisconsin 53706 and ‡Department of Biochemistry, University of Louisville, Louisville, Kentucky 40202 USA

ABSTRACT Ca^{2+} sparks are miniature Ca^{2+} release events from the sarcoplasmic reticulum of muscle cells. We examined the kinetics of Ca^{2+} sparks in excitation-contraction uncoupled myotubes from mouse embryos lacking the β_1 subunit and *mdg* embryos lacking the α_{1S} subunit of the dihydropyridine receptor. Ca^{2+} sparks occurred spontaneously without a preferential location in the myotube. Ca^{2+} sparks had a broad distribution of spatial and temporal dimensions with means much larger than those reported in adult muscle. In normal myotubes ($n = 248$ sparks), the peak fluorescence ratio, $\Delta F/Fo$, was 1.6 ± 0.6 (mean $\pm$ SD), the full spatial width at half-maximal fluorescence (FWHM) was 3.6 ± 1.1 μm and the full duration of individual sparks, Δt, was 145 ± 64 ms. In β-null myotubes ($n = 284$ sparks), $\Delta F/Fo = 1.9 \pm 0.4$, FWHM $= 5.1 \pm 1.5$ μm, and $\Delta t = 168 \pm 43$ ms. In *mdg* myotubes ($n = 426$ sparks), $\Delta F/Fo = 1 \pm 0.5$, the FWHM $= 2.5 \pm 1.1$ μm, and $\Delta t = 97 \pm 50$ ms. Thus, Ca^{2+} sparks in *mdg* myotubes were significantly dimmer, smaller, and briefer than Ca^{2+} sparks in normal or β-deficient myotubes. In all cell types, the frequency of sparks, $\Delta F/Fo$, and FWHM were gradually decreased by tetracaine and increased by caffeine. Both results confirmed that Ca^{2+} sparks of resting embryonic muscle originated from spontaneous openings of ryanodine receptor channels. We conclude that dihydropyridine receptor α_{1S} and β_1 subunits participate in the control of Ca^{2+} sparks in embryonic skeletal muscle. However, excitation-contraction coupling is not essential for Ca^{2+} spark formation in these cells.

INTRODUCTION

In response to cell depolarization, activation of dihydropyridine receptors (DHPR) promote the opening of ryanodine receptors (RyR) in the sarcoplasmic reticulum (SR) of muscle cells and this results in a transient elevation of cytosolic Ca^{2+}. The DHPR is formed by α_1, β, α_2/δ, and, in skeletal muscle, γ subunits. Depending on the DHPR α_1 subunit isoform, Ca^{2+} transients may be initiated by Ca^{2+} entry into the cell or triggered by charge movements in the α_1 subunit (Garcia-Martinez et al., 1994). Both mechanisms make use of the strict colocalization of DHPRs and RyRs that takes place in the junctional domains established between the transverse tubular system and the SR and in embryonic muscle, the surface membrane and the SR (Takemura et al., 1994; Carl et al., 1995; Protasi et al., 1996).

The Ca^{2+} transient triggered by depolarization originates from Ca^{2+} sparks, which are highly localized releases of Ca^{2+} from the SR due to the rapid opening and closing of a small number of RyR channels (Cheng et al., 1993). These release events are too small to lead directly to cell contraction. However, many properties of the Ca^{2+} sparks suggest they represent the elementary Ca^{2+} release events underlying muscle contraction (Cheng et al., 1993; Cannell et al., 1995; Tsugorka et al., 1995; Shacklock et al., 1995; Klein et al., 1996; Parker et al., 1996; Blatter et al., 1997). A whole-cell Ca^{2+} transient may thus result from the sum total of many Ca^{2+} sparks activated by voltage in junctional domains throughout the cell. In addition, Ca^{2+} sparks have been reported to occur at resting potentials (Cannell et al., 1995; Klein et al., 1996; Parker et al., 1996). In cardiac muscle, Ca^{2+} spark occurrence is consistent with a model in which membrane voltage recruits sparks in direct proportion to the number of activated L-type Ca^{2+} channels (Santana et al., 1996). The low open probability of the L-type channel at resting potentials could therefore account for the low frequency of Ca^{2+} spark observed in cardiac muscle at rest. In adult skeletal muscle, resting Ca^{2+} spark frequency was much higher than that predicted by the level of activation of voltage sensors at rest (Klein et al., 1996). The high occurrence and their persistence in the presence of nifedipine indicated that resting Ca^{2+} sparks in skeletal muscle are regulated by factors other than voltage. Consistent with this notion, resting spark frequency in frog muscle was shown to increase with cytosolic Ca^{2+} or low concentrations of caffeine (Klein et al., 1996). These results suggest that Ca^{2+} sparks in resting skeletal muscle originate from the openings of groups of RyR channels under the influence of cytosolic ligands.

The mechanisms that trigger the sudden opening of RyR channels to produce a Ca^{2+} spark and limit Ca^{2+} release to a few milliseconds are presently unknown. In skeletal muscle, the participation of DHPRs in the control of Ca^{2+} sparks is expected because interactions between DHPRs and RyRs account for many features of the macroscopic Ca^{2+} transient (Rios et al., 1991). In the present study we characterized Ca^{2+} sparks in embryonic mammalian skeletal muscle cells lacking either the α_{1S} or β_1 subunit of the

Received for publication 28 July 1998 and in final form 13 October 1998.
Address reprint requests to Roberto Coronado, Department of Physiology, University of Wisconsin, 1300 University Avenue, Madison, WI 53706. Tel.: 608-263-7487; Fax: 608-265-5512; E-mail: coronado@physiology.wisc.edu.

0006-3495/99/02/657/13 $2.00

DHPR. Both types of myotubes are excitation-contraction (EC) uncoupled due to the selective absence of either subunit from the DHPR (Adams et al., 1990; Tanabe et al., 1990; Garcia et al., 1994; Gregg et al., 1996; Strube et al., 1996; Beurg et al., 1997; Strube et al., 1998). We found that spontaneous Ca^{2+} sparks were highly abundant in these mutant cells, demonstrating that EC coupling is not essential for Ca^{2+} spark occurrence. Furthermore, the fact that Ca^{2+} spark properties in α_{1S} and β_1 deficient muscle cells are highly dissimilar raises the possibility that DHPR subunits may separately regulate RyRs under conditions in which the DHPR voltage sensor is nonfunctional. Some of these results were previously published in abstract form (Conklin et al., 1997, 1998a).

MATERIALS AND METHODS

Single cell preparation

All experiments were performed with freshly isolated intercostal myotubes from 18-day-old mouse fetuses (E18) as described elsewhere (Strube et al., 1996). Homozygotes for the *mdg* allele *(mdg/mdg)* and homozygotes for the β_1 mutation (*cchbl*$-/-$) are hereafter called *mdg* and β-null, respectively. Mice with a normal phenotype, hereafter called normal, were heterozygotes for either mutation *(mdg*/+ or *cchbl*$-/+$*)* or wild-type. The two half-ribcages of each fetus were dissected in normal Krebs solution containing 136 mM NaCl, 5 mM KC1, 2 mM $CaCl_2$, l mM $MgCl_2$, and 10 mM HEPES titrated to pH 7.4 with NaOH. The tissues were incubated at 37°C for approximately 10 min in phosphate buffered saline (Sigma Chemical, St. Louis, MO) containing collagenase (3 mg/ml, Type I, Sigma) and trypsin (1 mg/ml, Type III, Sigma). Single myotubes were obtained by mechanical dispersion. Isolated cells were allowed to settle in a culture dish with the bottom replaced by a thin glass coverslip for at least 1 hour before imaging. Myocytes were viable for several hours as demonstrated by their ability to produce Ca^{2+} sparks, maintain a relatively constant resting fluorescence, contract in response to caffeine, and, in the case of normal cells, contract in response to field stimulation. The SR Ca^{2+} loading was the same in all cell types as demonstrated by the amplitude of caffeine-induced Ca^{2+} transients.

Cell imaging

Cells were loaded with 2 μM fluo-3 acetoxymethyl (AM) ester (Molecular Probes, Eugene, OR) for 30 to 60 min at room temperature in Krebs solution. During imaging, cells were kept in Krebs solution without fluo-3 (AM) at room temperature. The total number of imaged cells in this study were 123 normal cells from 23 embryos, 23 β-null cells from 11 embryos, and 25 mdg cells from 8 embryos. To collect a large number of sparks under equivalent conditions, sites producing sparks were subjected to a maximum of 10 to 12 line scans equivalent to a total scanning time of 22 to 26 seconds per site. Considering scans with at least one spark, the mean frequency of spark occurrence was 1.6, 1.8, and 2.7 sparks per 2.2-second scan for normal, β-null, and mdg myotubes. Considering the cell dimension, the frequencies of sparks in line scans with at least one spark were 13, 15, and 22 $\times$ 10^{-3} sparks/s/μm, respectively.

Fluorescence confocal microscopy

Cells were viewed with an inverted microscope with a 40$\times$ oil immersion objective (N.A. = 1.3). The confocal attachments were either a Fluoview (Olympus, Melville, NY) or an MRC-1000 (BioRad, Hercules, CA). The 488 nm spectrum line necessary for fluo-3 excitation was provided by a 5 mW Argon laser or a 15 mW Krypton/Argon laser, respectively. The laser power was attenuated to between 6% and 30% with neutral density filters. The dimensions of the line scan images were 512 or 768 pixels/line with a pixel size of 0.1 $\times$ 0.1 to 0.3 $\times$ 0.3 μm and 512 to 1000 lines/image. The *z* axis resolution was ~0.8 μm and was estimated by imaging subresolution fluorescent beads (Molecular Probes). Image intensity was digitized at a resolution of 8 bits in the BioRad scanner and 12 bits in the Fluoview scanner. The line scan rate was calibrated with a light-emitting diode and a voltage pulse from a digital pulse generator. The line scan rate was 4.3 ms per 768-pixel line in the BioRad scanner and 2.05 ms per 512-pixel line in the Fluoview scanner.

Ca^{2+} spark analysis

Ca^{2+} sparks were initially identified in two-dimensional images and afterwards acquired in line-scan mode. For line-scan acquisition, the confocal plane and the line position were adjusted to achieve maximum image resolution. We investigated if the shape of the spark varied when sites were scanned longitudinally versus transversely as shown in adult cardiac myocytes (Parker et al., 1996). This was not the case and therefore, no efforts were made to orient the cell relative to the scan direction. Individual sparks were identified by an experimenter according to the following criteria. A single event corresponded to a transient elevation in intensity $>$ 0.3 ΔF/Fo units with a full spatial width $>$ 1 μm and a full duration $>$ 10 ms and $<$ 350 ms. The full duration was the time interval during which the fluorescence remained elevated $>$ 0.3 ΔF/Fo units above the mean baseline fluorescence. This definition excluded fused events occurring in rapid succession in cases in which the background fluorescence between sparks could not be adequately measured. Using these criteria, the smallest Ca^{2+} spark identified had a spatial width of 10 pixels, a full duration of 15 pixels and a fluorescence intensity $>$ 30% above the average resting intensity of the image. Many cells produced spatially small and large sparks at the same location. In these cases, small sparks could not be explained by out-of-focus fluorescence for two reasons. First, we varied the *z*-plane a few microns in both directions and did not detect an increase in the spatial width of small sparks. Second, the bulk of the small sparks was detected in *mdg* myotubes, which suggested they were cell-specific events. To produce an average spark image, we used National Institutes of Health-Image 1.6 (National Institutes of Health Public Software Library). A small frame of fixed dimensions (typically 15 μm $\times$ 400 ms) was moved laterally and vertically in a line scan until the peak fluorescence of a spark coincided with the center of the frame. The section of the line-scan image within the boundaries of the frame was copied to a new image. The latter images, all of identical size and each of a single spark, were placed in a stack and averaged. When appropriate, the cytosolic free Ca^{2+} was calculated with the equation $[Ca^{2+}]i = Kd\ (F/Fo)/[Kd/([Ca^{2+}]_{rest} + 1) - (F/Fo)]$, assuming a Kd for Ca-fluo of 1.1 μM and a nominal resting free Ca^{2+} concentration, $[Ca^{2+}]_{rest}$, of 100 nM (Shirokova et al., 1996). The fluorescence intensity, F, was calculated by densitometric scanning of Ca^{2+} sparks in line-scan images. To improve the signal-to-noise ratio, F was averaged over 10 pixel lines nearest to the center of sparks. The fluorescence intensity, Fo, was averaged in the same manner from areas of the same image without sparks. The fluorescence unit, ΔF/Fo, was constructed by subtracting unity from the ratio F/Fo. A compressed 32-color table and an 8-pixel running average (smoothing) was applied to all images to highlight the center of the spark. The pixel intensity shown in scans of fluorescence as a function of time and space was obtained directly from the bit-map file with tools provided by National Institutes of Health-Image 1.6 or IDL 5.0 (Research Systems, Inc., Boulder, CO).

Chemicals

A 1-mg sample of fluo-3 AM (Molecular Probes) was dissolved in 1 ml of DMSO and kept frozen until use. Stock solutions of tetracaine and caffeine (Sigma), 4 mM and 10 mM respectively, were prepared in glass-distilled water.

RESULTS

The *mdg* and β-null myotubes are EC-uncoupled and do not produce intracellular Ca^{2+} transients in response to cell depolarization (Tanabe et al., 1990; Gregg et al., 1996). Therefore, to compare Ca^{2+} sparks of normal and mutant cells side by side, measurements were made at rest. Fig. 1 shows sections of intercostal myotubes in which a Ca^{2+} spark was captured during the acquisition of a two-dimensional image. Dissociated myotubes were typically ~200 μm in full length and ~15 μm in maximum width. Ca^{2+} sparks engulfed a significant fraction of the cell width and tended to repeat themselves at the same location. However, the location of sparks within cells bared no obvious relation to the few recognizable morphological features revealed by the fluo-3 staining pattern such as the perinuclear region or the center or tips of cells. Although highly variable, myotubes actively engaged in formation of sparks typically had one to three simultaneously active sites per cell. In addition, there were numerous silent cells, especially among normal cells, in which sparks were not produced. The frequency of sparks in active sites was relatively low. Considering those line scans with at least one spark, the spark frequencies were roughly 10×10^{-3} to 20×10^{-3} events/μm/s (see Materials and Methods).

Sites of Ca^{2+} sparks identified in 2-D images were subjected to repetitive line scans. Many myotubes showed time-invariant fluorescence, most commonly in the nuclear and perinuclear regions. These regions were carefully avoided. Fig. 2 *A* shows line-scan images of Ca^{2+} sparks in β-null myotubes. Time increases from left to right and the spatial dimension is vertical. Only the cell region covered by the spark is shown in the image. A trace of fluorescence intensity as a function of time near the center of all sparks is shown next to each line-scan image (Fig. 2 *B*). Similar to reports in normal adult cells, Ca^{2+} sparks in β_1-null cells originated from sudden increases in fluorescence followed by a slower return of the signal to baseline. However, many events in β-null cells had a characteristic slow onset such that the time to peak was similar to the time elapsed between peak and decay to baseline. Also noticeable was the fact that the spatial width was much larger than previously described in adult cardiac or skeletal muscle cells (Parker et al., 1996; Lacampagne et al., 1996). Both features, namely the time to peak and the width, are described below for mutant and normal cells.

Most sparks in β_1-null cells were spatially symmetrical. However, there were occasional asymmetrical or skewed events. Examples of the latter kind are the last two sparks in the uppermost line scan of Fig. 2 *A*. Within these sparks, the fluorescence spreads preferentially toward the bottom and in the next event preferentially toward the top of the image. This is better appreciated in Fig. 3, where the spatial fluorescence intensity of each of the two sparks in question (panels *B* and *C*, respectively) is shown every 30 ms, starting from the background intensity before each event. The left end of each trace in Fig. 3 corresponds to the top end of the line scan. The spatial fluorescence moved preferentially from left to right in panel *B*, from right to left in panel *C*, and more or less evenly in both directions in panel *A*, which corresponds to the first spark in the same line scan. Furthermore, the initial fluorescence increase occurred at a slightly different location in each case. This is indicated in Fig. 3 by the location of the peak fluorescence in trace 2 of each panel. Thus, a Ca^{2+} spark in β_1-null cells could be initiated by one of several closely spaced Ca^{2+} release sites. Once activated, other locations nearby became progressively activated. This model is further described below in the Discussion section. Skewed sparks were relatively frequent in β_1-null cells and were seldom seen in *mdg* or normal myotubes.

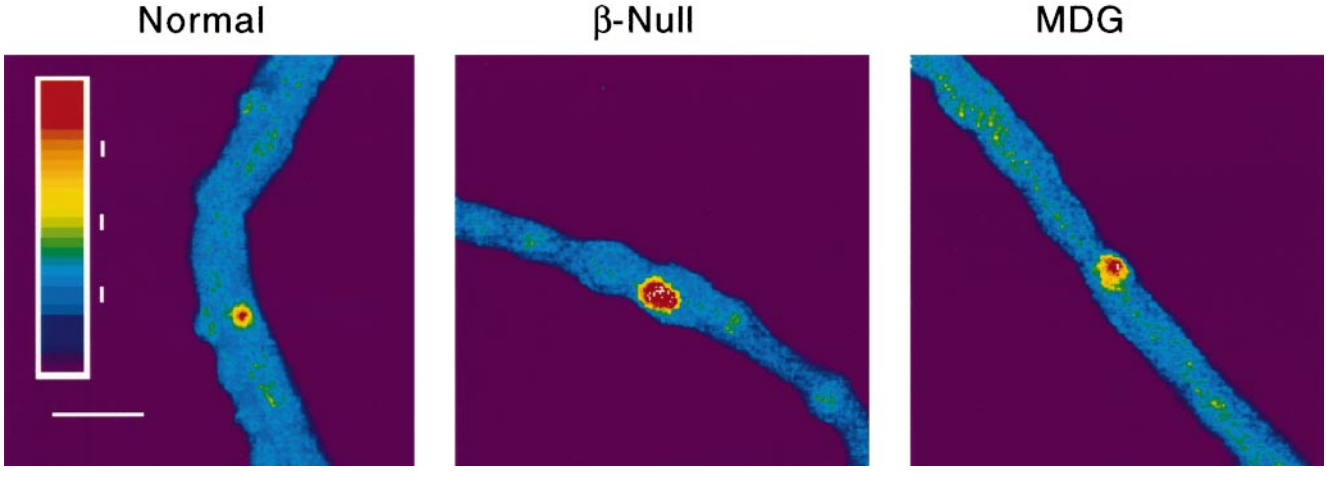

FIGURE 1 Two-dimensional images of Ca^{2+} sparks in normal and mutant embryonic myotubes. Images have a size of 512 × 512 pixels (0.2 × 0.2 μm per pixel) and were acquired at a rate of 1.05 s per image. An 8-pixel smoothing and a 32-color table were applied to highlight Ca^{2+} spark location. The background of the image, containing debris and other cells, was removed. The rainbow color scale is applicable to this and all other figures. Indicated are narrow ranges of color representing ΔF/Fo = 0, 1, and 2. The scale bar is 23 μm and is the same for the three cell types.

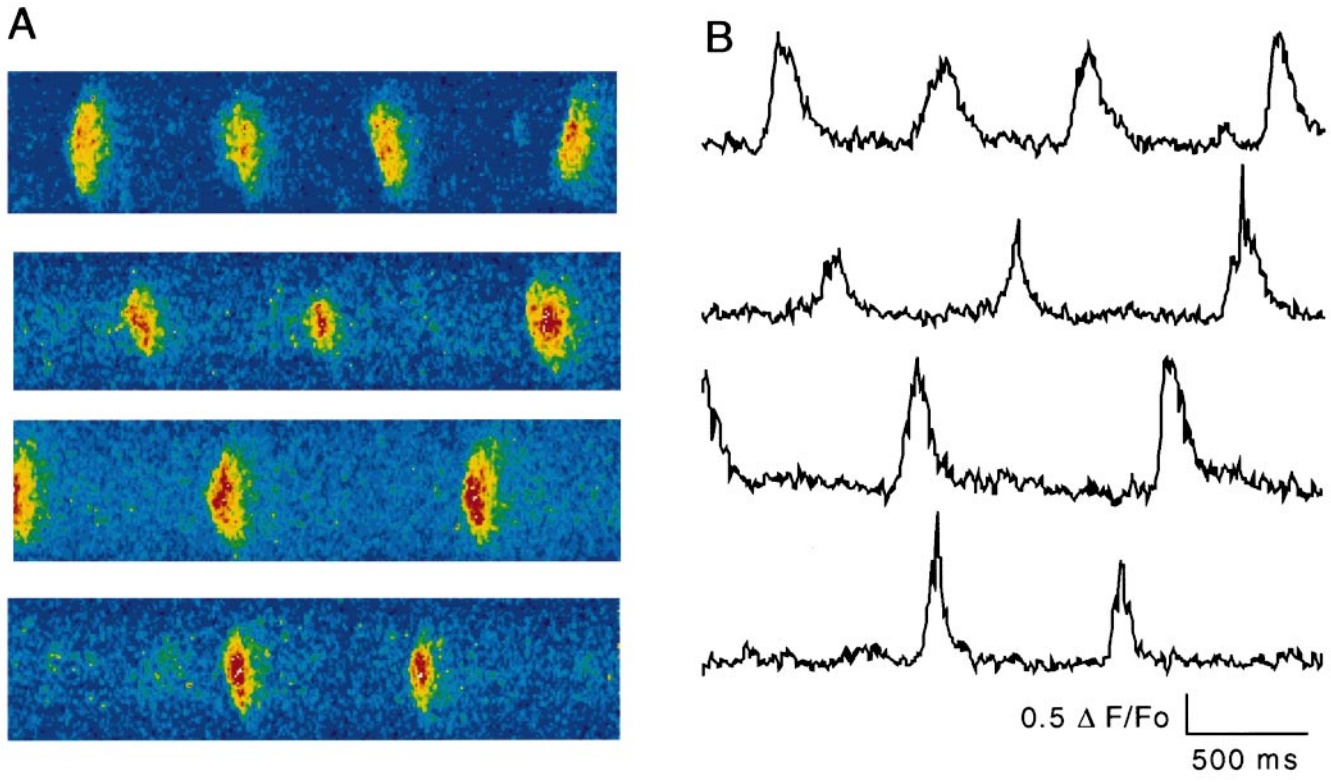

FIGURE 2 Line-scan images of Ca^{2+} sparks in β-null myotubes. Images have a size of 22 μm (vertical) $\times$ 2.2 s (horizontal) and a pixel size of 0.22 μm $\times$ 4.3 ms. Each image is from a different myotube. The time course of fluorescence intensity through the center of the sparks is shown for each line scan.

Occasionally, a site in a β_1-null myotube produced Ca^{2+} sparks at a relatively high rate for several minutes. We took advantage of this phenomenon to expose cells to illumination for a prolonged period and thus determine the extent to which multiple scans of the same location altered the properties of the Ca^{2+} sparks at that location. Fig. 4 shows the average time course and the spatial spread of fluorescence of 49 events from the same location in a β-null cell captured in 20 line scans. In this experiment, the total line-scan time was 44 s, approximately twice the typical scan time per site (see Materials and Methods). In addition to the relatively constant spark frequency, this site was chosen because all the sparks were homogeneous in shape and size; therefore, intrinsic time-dependent changes unrelated to the history of illumination were minimized. The images (panel *A*) and the densitometric scans (panels *B* and *C*) correspond to averages of 10 sparks (except the bottom image) arranged consecutively in time from top to bottom. The time interval between the images was ~150 s. The traces indicated that the kinetics of onset and decay as well as the spatial width of sparks remained remarkably constant during this period. These results showed that deleterious effects usually associated with repetitive line-scan imaging, such as dye bleaching and photodamage, were not critical limiting factors in our measurements.

Line scans of Ca^{2+} sparks in *mdg* myotubes are shown in Fig. 5 *A* at the same magnification used for β-null cells. Events in *mdg* cells were much more heterogeneous than those in β-null cells. There were Ca^{2+} sparks of the same spatial dimension as those of β-null and, in addition, a subset of sparks that were noticeably smaller in size, duration, and brightness. Evidently, large and small sparks originated from the same cellular location. This was most obvious in the second line scan from the top in Fig. 5 *A*. The traces of signal intensity as a function of time (Fig. 5 *B*) showed that the majority of sparks in these cells, unlike those in β-null cells, had a sharp rising edge followed by a much slower decline toward baseline. The latter are stereotypical kinetic features of Ca^{2+} sparks of adult cells. Histograms of the full spatial width at half-maximal fluorescence (FWHM), the maximum fluorescence intensity ($\Delta F/Fo$), and the event duration (Δt) of sparks collected in normal (248 sparks from 116 cells), β-null (284 sparks from 15 cells), and *mdg* (426 sparks from 19 cells) myotubes are shown in Fig. 6. The larger number of normal cells reflects the fact that considerably fewer sparks were produced in these cells. Indicated in the figure legend are the mean ($\pm$ SD) of each of these distributions. For visual comparison, the gray bar in each histogram contains the population mean. The distributions were roughly symmetrical except for those of spark duration and fluorescence intensity in normal cells. In these cases, the smallest events were more frequent than expected assuming a normal distribution. The population averages of normal cells were slightly lower than

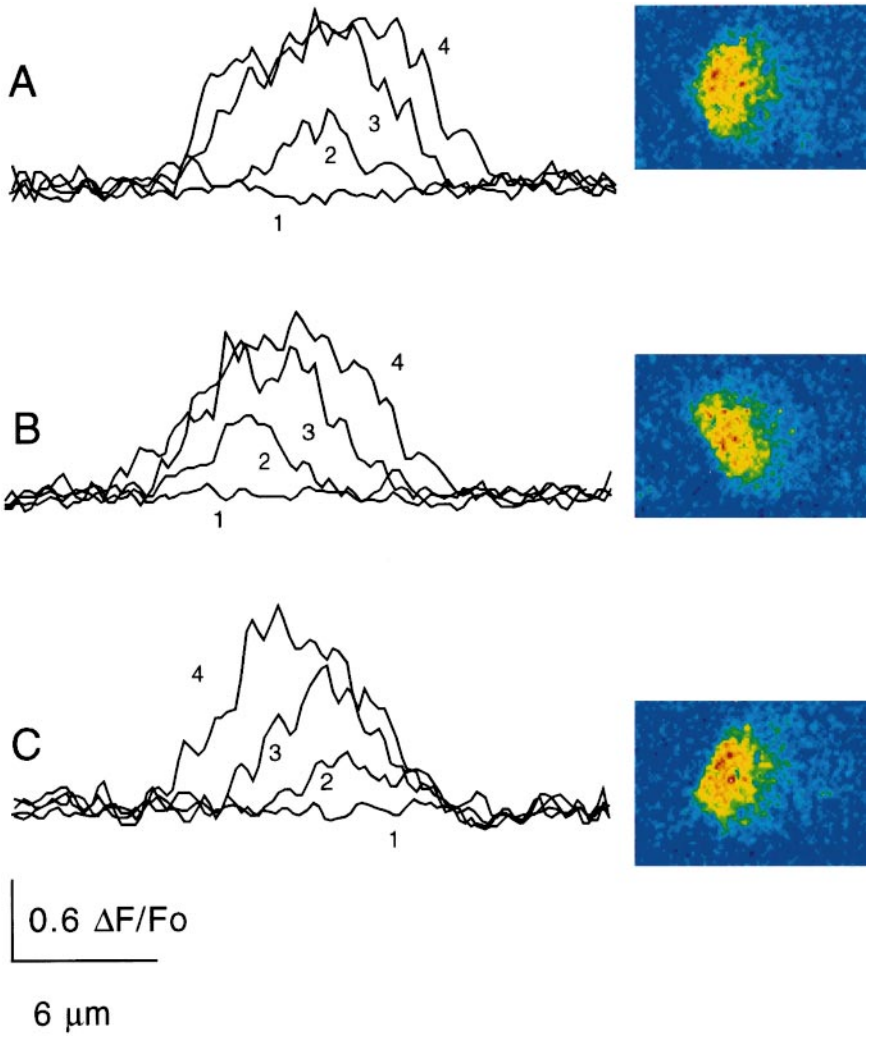

FIGURE 3 Spatial propagation of fluorescence in skewed Ca^{2+} sparks of β-null myotubes. Profiles of spatial fluorescence intensity at fixed times are shown for the first (*A*), third (*B*) and fourth or last (*C*) spark of the uppermost line scan of Fig. 2 *A*. These sparks are shown next to the spatial intensity profiles. The image size is 15.4 μm (vertical) by 430 ms (horizontal). The spatial intensity was averaged over seven lines starting with trace 1, which corresponds to the background intensity before any detectable increase in fluorescence. Profiles labeled 1 through 4 are separated by 30.1 ms with trace 4 close to the peak fluorescence.

those of β-null cells and significantly higher than those of *mdg* cells. Those of β-null cells were significantly higher than those of *mdg* cells (nonpaired *t*-test, $p < 0.05$). Nominal free Ca^{2+} concentrations at the maximum spark fluorescence were estimated assuming a resting free Ca^{2+} concentration of 100 nM (Shirokova et al., 1996) and were 206 ± 90, 245 ± 70, and 118 ± 72 for normal, β-null, and *mdg* cells, respectively. These estimates were higher than those of Tsugorka et al. (1995) and within range of those of Klein et al. (1996) in adult frog skeletal muscle. However, the Ca^{2+} buffering capacities of the internal solutions used in these studies were widely different (respectively, 10 mM versus 0.1 mM EGTA-Ca^{2+}). Hence a comparison between the published reports and the present study was difficult. In summary, these data showed that the specific absence of DHPR α_{1S} or β_1 subunits significantly influenced the spatial and temporal properties of Ca^{2+} sparks in embryonic muscle.

Because the parameters FWHM, ΔF/Fo, and Δt of individual sparks are not expected to behave entirely independently of each other, we plotted them in three dimensions (Fig. 7). The 3-D plots showed that there was a tendency for Ca^{2+} sparks to increase in intensity and dimension in parallel with an increase in duration. Accordingly, the shape of the 3-D distributions was roughly that of a broad ellipsoid extending through the middle of the dimension-intensity (*x*-*y*) plane and upwards along the duration (*z*) axis. However, in β-null cells there were numerous sparks for which peak fluorescence did not increase in proportion to the increase in spark width. The correlation between these parameters is better appreciated in the bottom panels of Fig. 7, in which events were sorted into bins. In the bottom 3-D graphs, the average FWHM and the average value of the other two parameters for events in the same bin were plotted, conserving the same axis as in the top graphs. The increase in spark width correlated with the increase in spark fluorescence and duration. The parameters of sparks in the two smallest bins for normal and β-null cells and four smallest bins in *mdg* cells were significantly smaller than those in the largest bin (nonpaired *t*-test, $p < 0.05$). To extend this correlation further, we grouped sparks into two populations so that we could compare what effects a doubling of spark width would produce in the other two parameters. A doubling of β-null spark width from $3.5 \pm$

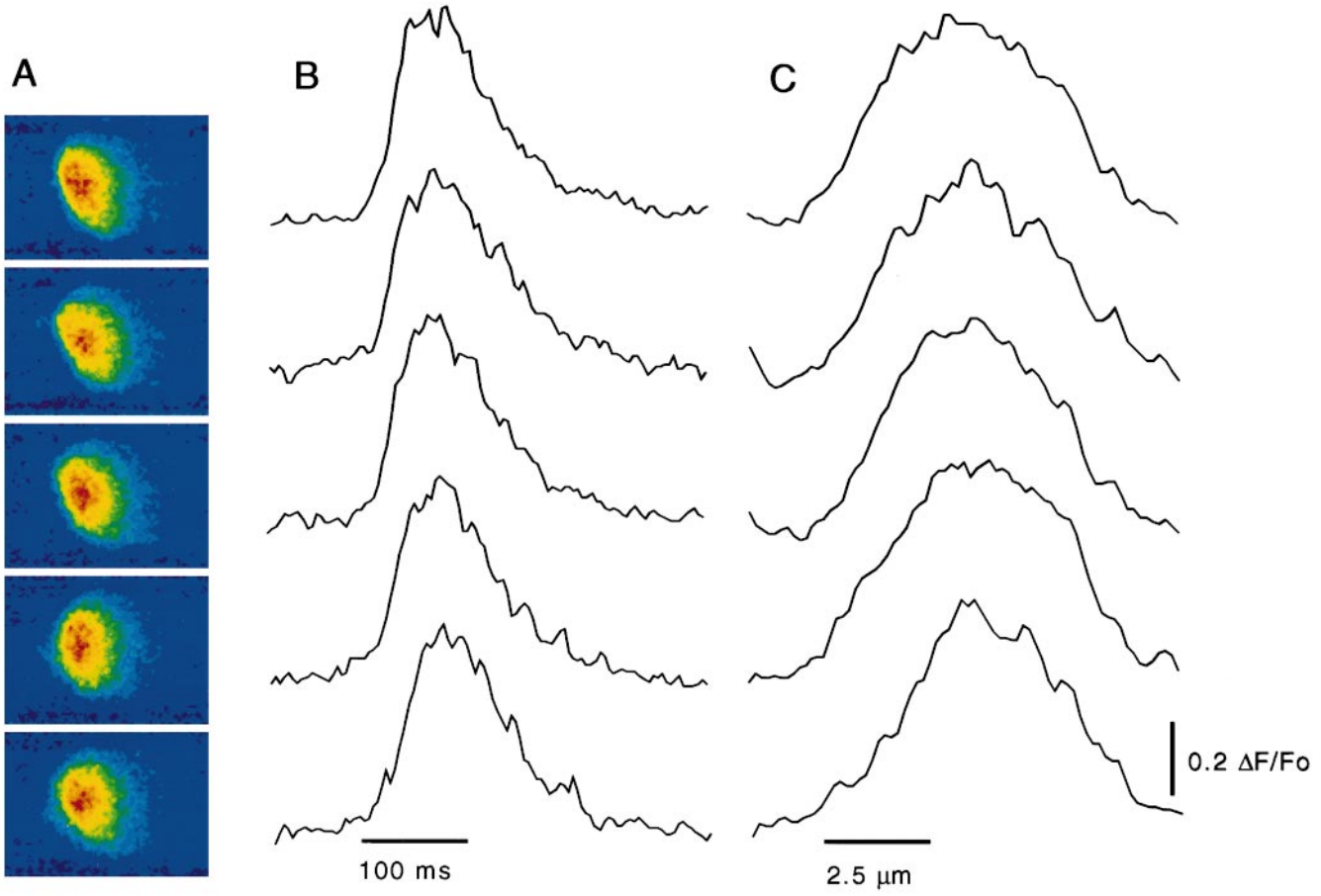

FIGURE 4 Time course and spatial dimension of repetitive sparks from the same location in a β-null myotube. *A* shows a total of 49 sparks acquired during a period of ~15 min. Each image from top to bottom is the average of 10 consecutive sparks (except the last image with 9 averaged sparks). The dimensions of each image are 15 μm (vertical) $\times$ 430 ms (horizontal) with a pixel size of 0.22 μm $\times$ 4.3 ms. The time course of fluorescence intensity in time (B) and space (C) passing through the center of the average spark is shown for each line scan.

0.034 to 7.4 $\pm$ 0.1 μm (n = 161) resulted in a modest change in fluorescence (1.65 $\pm$ 0.06 vs. 1.9 $\pm$ 0.03 ΔF/Fo) and duration (151 $\pm$ 5.4 vs. 178 $\pm$ 6 ms). In contrast, a doubling in *mdg* spark width from 1.9 $\pm$ 0.02 to 4.1 $\pm$ 0.09 μm (n = 153) resulted in a doubling in spark fluorescence (0.76 $\pm$ 0.03 vs. 1.44 $\pm$ 0.06 ΔF/Fo) and duration (84 $\pm$ 3 vs. 154 $\pm$ 6 ms). In normal cells, the result was intermediate. A doubling in normal cell width from 1.7 $\pm$ 0.08 to 3.5 $\pm$ 0.03 μm (n = 89) resulted in a modest change in spark fluorescence (1.26 $\pm$ 0.09 vs. 1.55 $\pm$ 0.06 ΔF/Fo) and a 1.4-fold increase in duration (110 $\pm$ 16 vs. 153 $\pm$ 7 ms). Thus, in *mdg* cells the spark half-width increased in proportion to the event fluorescence and the event duration, whereas in the other two cell types this correlation was weaker. Because the three parameters were strongly correlated at least in *mdg* cells, the broad range of spatial half-widths and intensities encountered in *mdg* cells could be secondary to the broad distribution of event duration measured in these cells from 26 ms to 300 ms. In contrast, we found that large sparks in β-null cells with a half-widths $>$ 4 μm all had roughly the same peak fluorescence. This suggests that the mechanism of formation of large sparks in β-null cell may be entirely different from those underlying small sparks in *mdg* cells.

Additional differences between the two mutant cells were found in the kinetics of spark formation. The left panel of Fig. 8 shows the time course of ΔF/Fo obtained from six separate sites, each in a different normal or mutant cell. All sparks in a site were aligned as described in Materials and Methods and the mean time course was computed from the average image. In order to include dim and bright average sparks, we normalized the mean time course from single sites according to the peak fluorescence and shifted the time courses in time so that the peak fluorescences coincided. The upper right corner of the rectangle drawn on top of each average corresponds to the peak fluorescence and the lower left corner corresponds to the time at which the fluorescence was 1 standard deviation higher than the mean baseline fluorescence. Thus, the time required for the average Ca^{2+} spark to reach maximum fluorescence was approximately equal to the base of the rectangle. These averages showed that the time required for sparks to reach their peak was much longer in β-null cells than in normal or *mdg* cells. The β-null averages resulted in a slowly rising waveform which

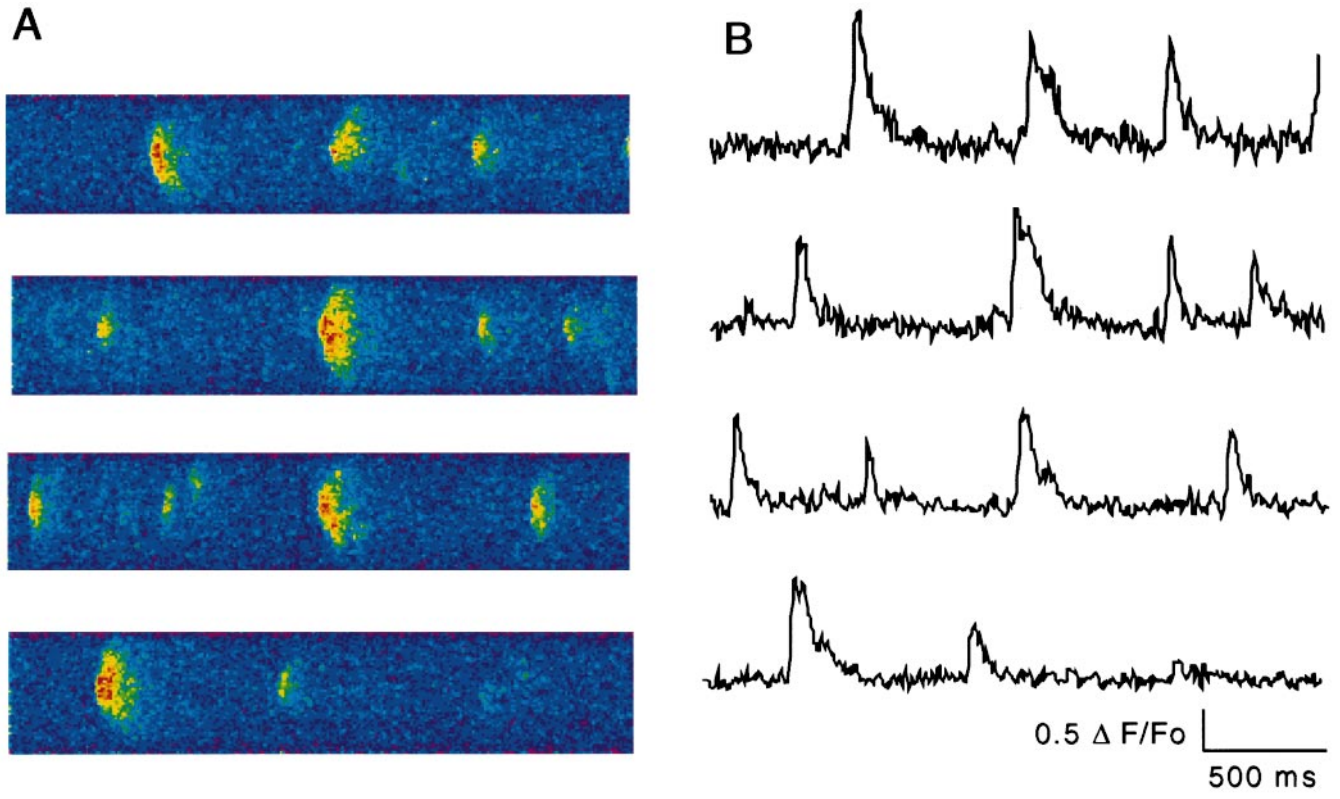

FIGURE 5 Line-scan images of Ca^{2+} sparks in *mdg* myotubes. Images have a size of 15 μm (vertical) $\times$ 2.2 s (horizontal) and a pixel size of 0.22 μm $\times$ 4.3 ms. Each image is from a different myotube. The time course of fluorescence intensity through the center of the sparks is shown for each line scan.

could have been exacerbated by averaging normalized dim and bright sparks. The right panel of Fig. 8 presents our computation of the time course of the rate of fluorescence change from the same sites without subjecting sparks to normalization. The maximum rate was significantly smaller in β-null cells than in normal or *mdg* cells. Averages are indicated in the figure legend. This result confirmed that the slow kinetics of Ca^{2+} increase during a spark was a true feature of events in β-null cells. Furthermore, when sparks were individually measured, the time to peak was 42 $\pm$ 1.5 ms (mean $\pm$ SD, $n = 248$) for normal, 58 $\pm$ 1.2 ms ($n = 284$) for β-null, and 22.6 $\pm$ 0.9 for *mdg* cells ($n = 426$) and any two means were significantly different (nonpaired *t*-test, $p < 0.05$). On the other hand, the decay times were approximately the same in all cases. Decay times could be fit by a single exponential with a time constant of $\sim$140 ms. Because diffusion of the Ca^{2+}-dye complex away from the site of Ca^{2+} release dominates the decline of the Ca^{2+} spark (Gomez et al., 1996), it was not surprising to find a similar spark decay time in all cases. The slower rate of fluorescence increase in β-null cells suggested that the recruitment of open RyR channels was a much slower process in these cells.

Conceivably, a Ca^{2+} spark could arise from Ca^{2+} influx into the cell caused by long openings of L-type Ca^{2+} channels, which are known to be present in the mutant cells (Strube et al., 1998). This possibility was discarded because Ca^{2+} sparks were observed in the presence of the Ca^{2+} channel blockers as well as in cells without external Ca^{2+} (not shown). To determine if sparks originated from Ca^{2+} release mediated by RyRs, we treated cells with caffeine and tetracaine, which are known to affect RyRs and respectively to stimulate and inhibit Ca^{2+} sparks in adult muscle (Klein et al., 1996; Shirokova and Rios, 1997). Fig. 9 shows line scans in cells during a control period and 5 min after addition of 10 μM caffeine to the bath. This concentration of caffeine was found to produce changes in spark appearance without changes in the cell background. At higher concentrations (100 μM, see Fig. 10), caffeine increased the background fluorescence and made the identification of sparks difficult. As shown in Fig. 9, caffeine in the low micromolar range produced a marked increase in peak fluorescence and increased the time required for recovery of the rest fluorescence after release. Sparks had a characteristic comet-like shape consisting of a prolonged decay phase. This tail of fluorescence increased the overall duration of the events in these experiments by $\sim$30% in normal cells and 10–15% in the mutant cells. However, in these conditions we did not detect an increase in event frequency, which in adult cells has been shown to occur at a much higher caffeine concentration (Klein et al., 1996). The inhibitory effect of tetracaine is shown in Fig. 10. From top to bottom, the panels show line scans in cells during a control period (panel *A*), 10 min after addition of 0.2 mM tetracaine

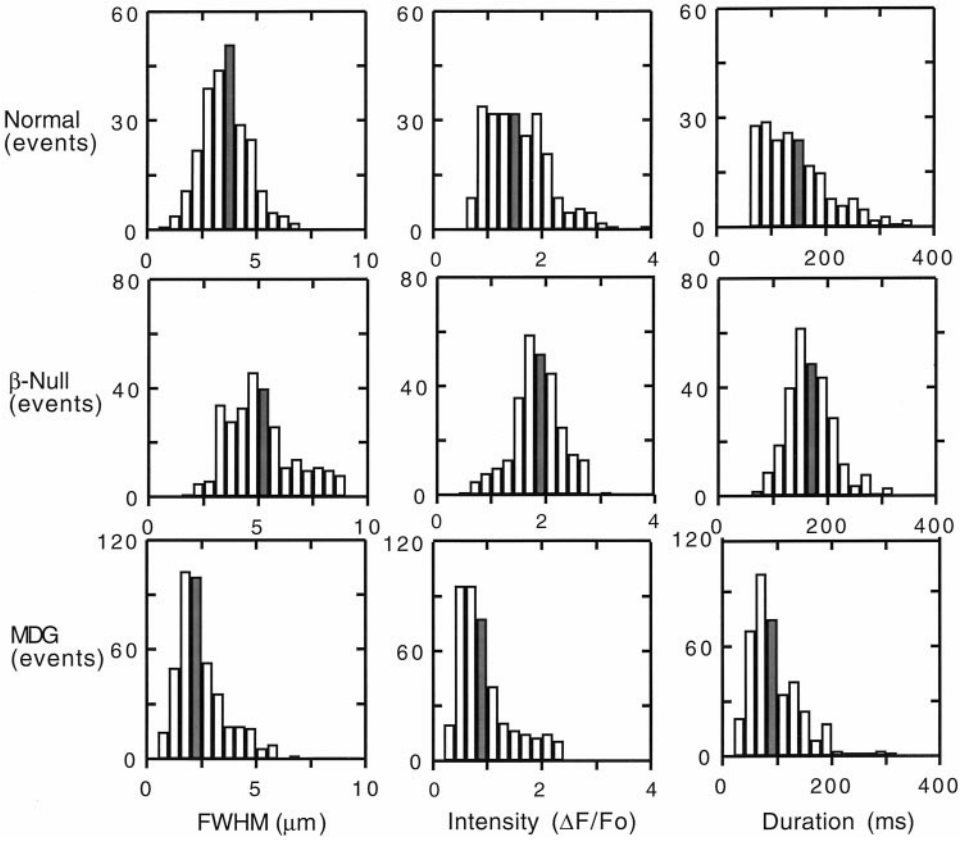

FIGURE 6 Histograms of Ca^{2+} spark size, intensity and duration. The FWHM, ΔF/Fo, and duration of individual Ca^{2+} sparks identified in normal (248 sparks), β-null (284 sparks), and *mdg* (426 sparks) myotubes were sorted into 20 bins. For each spark parameter, the abscissa (bin scale) is the same for all cell type. For each cell type, the ordinate (events/bin) is the same for all spark parameters. The mean of each distribution is included in the gray bar. The mean (± SD) for distributions of FWHM were, in microns, 3.6 ± 1.1, 5.1 ± 1.5, and 2.5 ± 1.1 for normal, β-null, and *mdg* cells, respectively. Those for distributions of ΔF/Fo were 1.6 ± 0.6, 1.9 ± 0.4, and 1 ± 0.5; those for distributions of Δt were, in milliseconds, 145 ± 64, 168 ± 43, and 97 ± 50, respectively.

to the bath (panel *B*) and 30 min after exposure of the cells to tetracaine (panel *C*). The brief exposure to tetracaine resulted in a clear decrease in spark width and intensity. After the prolonged exposure, Ca^{2+} sparks ceased to occur entirely and the inhibition could not be reversed after extensive washout of tetracaine. To ensure that the loss of activity was not due to a loss in SR Ca^{2+}, we exposed the same cells to 0.1 mM caffeine (panel *D*). There was a rapid increase in line-scan fluorescence; however, the recovery of Ca^{2+} spark activity was difficult to assess under these conditions. The results shown in Figs. 9 and 10 showed that Ca^{2+} sparks in embryonic muscle were indeed mediated by RyR channels. Additional experiments (not shown) demonstrated that sparks ceased to occur after treatment of cells with thapsigargin (1 μM) or ryanodine (10 μM), which agrees with the same conclusion.

DISCUSSION

The present study showed that spontaneous Ca^{2+} sparks are present in embryonic muscle and these events are due to Ca^{2+} release from the SR mediated by RyRs. Sparks in DHPR α_{1S}-deficient myotubes were significantly dimmer, smaller, and briefer than those in β_1-deficient or normal myotubes. To identify possible mechanisms involved in Ca^{2+} spark formation in embryonic myotubes, we compared Ca^{2+} spark parameters in embryonic and resting adult cardiac and skeletal muscle. Spontaneous Ca^{2+} sparks in resting adult cardiac muscle (Cheng et al., 1993; Cannell et al., 1995; Gomez et al., 1996) had a peak fluorescence F/Fo of ~2 (ΔF/Fo~1), a decay half-time of ~20 ms (equivalent to an estimated full-time duration of ~60 ms) and a spatial FWHM of ~1.9 μm. Ca^{2+} sparks in frog adult skeletal muscle had the same characteristics at all potentials, including a peak ΔF/Fo of ~1, a decay half-time of ~15 ms (equivalent to a full-time duration of ~45 ms), and a FWHM of ~1.5 μm (Lacampagne et al., 1996). The parameters of Ca^{2+} sparks in the three types of embryonic myotubes investigated (Fig. 6) were broadly distributed with population means significantly larger than those listed above for adult muscles. In particular, the kinetics of spark decay were threefold to sixfold slower and the spatial widths were 1.5-fold to twofold larger than in adult cells. Because the spatial half-width, particularly in β-null myotubes, varied between 3 and 7 μm, we considered the possibility that large events in these cells may have originated by summation of two smaller events. If this were the case, the mean intensity of the conspicuously large sparks should be significantly higher than that of sparks half their size. Calculations showed that in the range of 3.5–7.5 μm, sparks of β-null myotubes had approximately the same intensity, a feature also seen in the 3-D representation of the same data. Also, the distribution of half-widths and intensity for all cell types were broad but gave little indication of the presence of multiple maxima, which would be indicative of a unit and multiples of a unit. We are thus inclined to

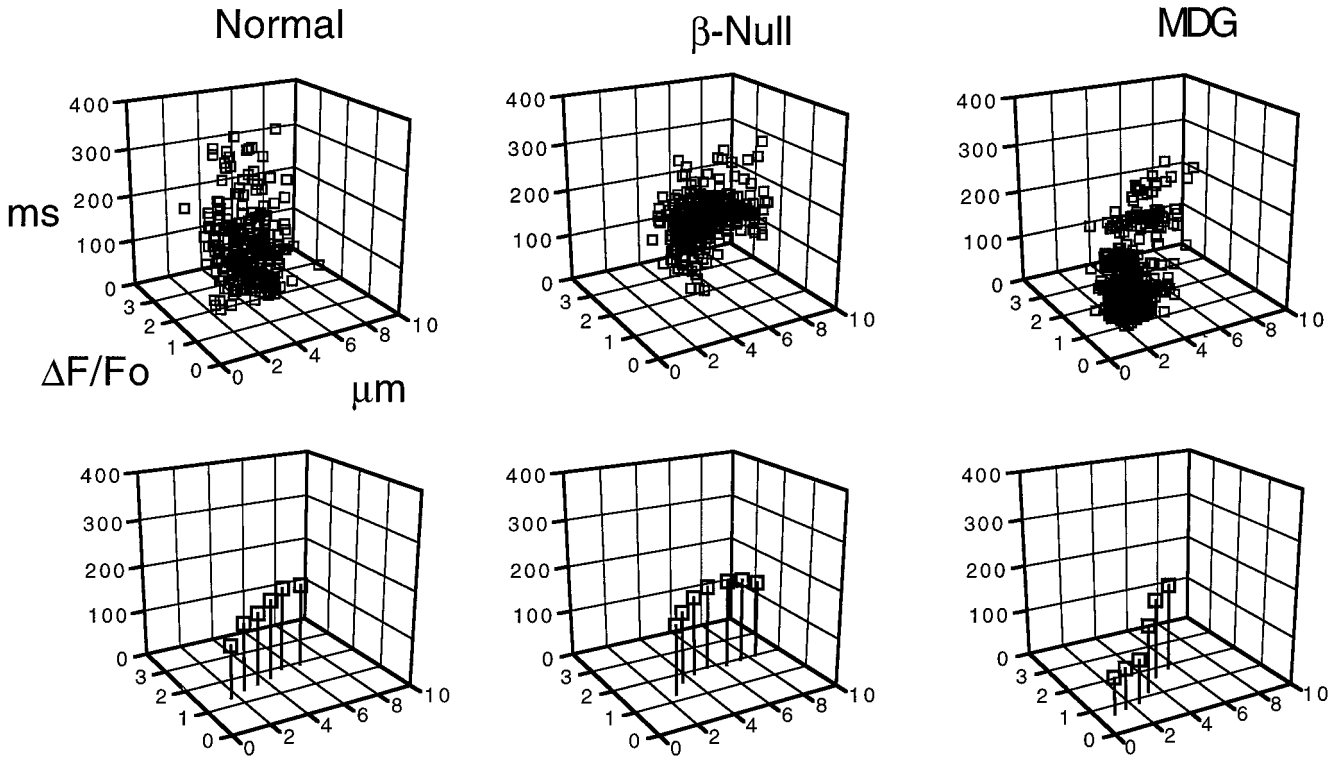

FIGURE 7 Relation of Ca^{2+} spark width to intensity and duration. The FWHM (*x* axis), ΔF/Fo (*y* axis) and duration (*z* axis) of Ca^{2+} sparks in normal (248 sparks), β-null (284 sparks), and *mdg* (426 sparks) myotubes appear in the top panels in graphs in three dimensions. The bottom graphs reflect the same data averaged within bins. The mean FWHM, ΔF/Fo, and Δt in each bin is indicated by the square symbol. The line is a drop to the *x-y* plane. The axis labels are the same for all graphs and were removed for clarity.

believe that the basis for the heterogeneity of spark parameters seen in the present study may reside elsewhere. We suggest that large sparks in the β-null cell are produced by activation of large clusters of Ca^{2+}-gated RyRs (Fig. 11). The spatial spread of fluorescence in the large spark would involve, in addition to Ca^{2+}-dye diffusion away from the

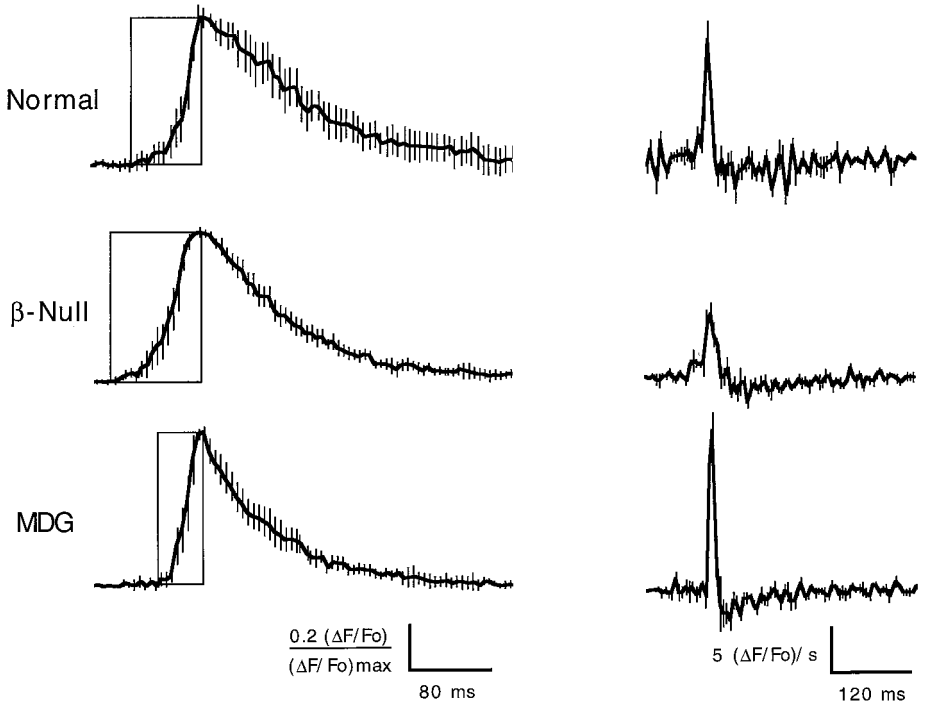

FIGURE 8 Mean time course of Ca^{2+} sparks in normal, β-null and *mdg* myotubes. Left panel shows traces corresponding to the mean time course of fluorescence through the center of sparks from six different sites in *mdg* and β-null cells and five sites in normal myotubes. The traces were shifted so that the peak ΔF/Fo (ΔF/Fo max) coincided in all cases. Each trace was normalized according to ΔF/Fo max. The continuous line is the time course of the mean and the bar heights correspond to 2 standard deviations. The rectangle was drawn to indicate the beginning of the spark (*lower left corner*) and the time to peak fluorescence (*upper right corner*). The right panel shows the time course of the rate of fluorescence change, d(ΔF/Fo)/dt, computed for sites without normalization. The maximum rate of fluorescence change were, in (ΔF/Fo)/sec, were 13.3 ± 2, 7.2 ± 1.2, and 17.9 ± 2 for normal, β-null, and *mdg*, respectively. The maximum rate of β-null cells was significantly smaller than that of the other two myotube types (*t*-test, $p < 0.026$).

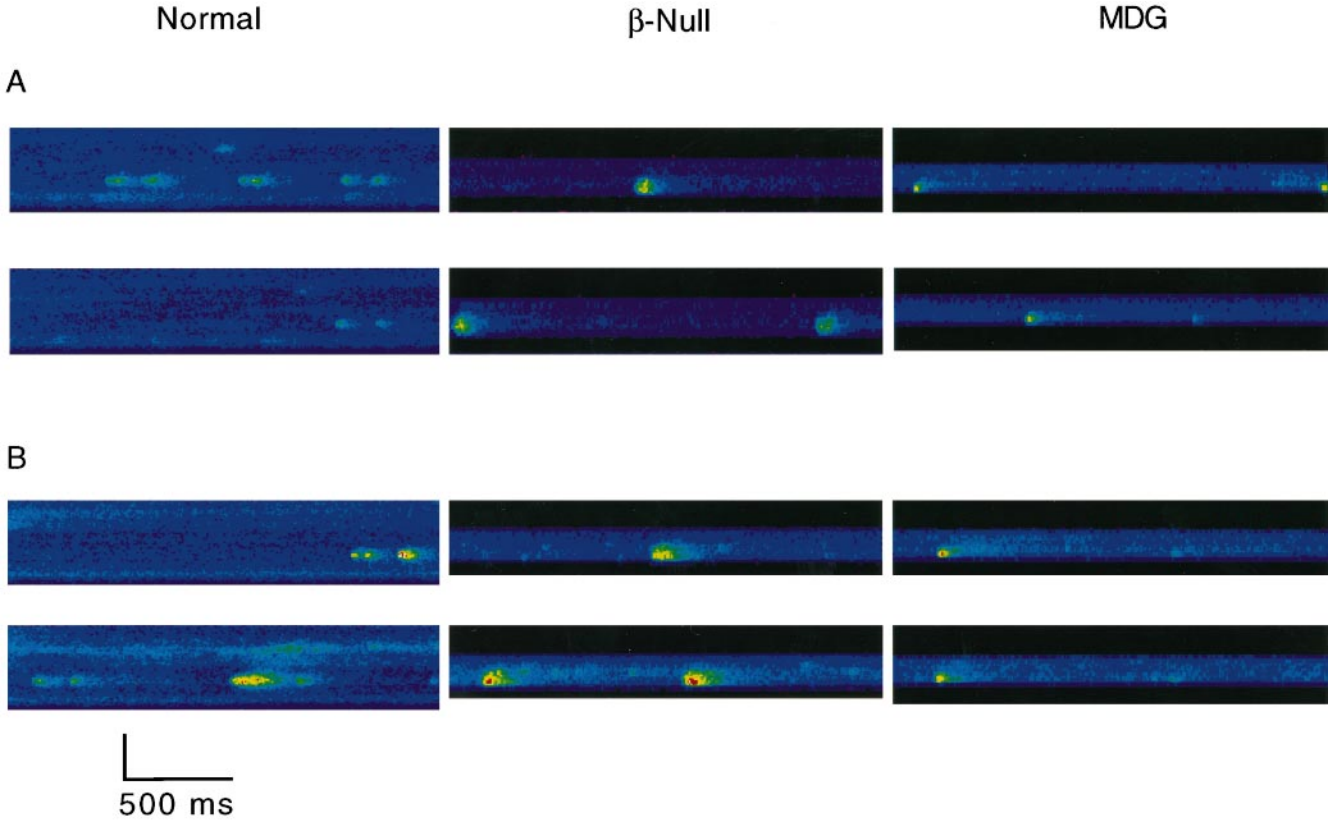

FIGURE 9 Stimulation of of Ca^{2+} sparks by caffeine. Panel *A* shows two line-scans from the same location in each cell during a control period. Panel *B* shows two line-scans of the same cell and location 5 min after addition of caffeine at a final concentration of 10 μM to the bath solution. The vertical scale bars are 20 μm for normal, 12 μm for β-null, and 10 μm for *mdg* myotubes.

center of the spark, successive activation of RyR channels in all directions within the cluster. The spread of fluorescence would be limited only by the size of the cluster. Such a mechanism would also explain the presence of skewed events. If a spark is initiated in the edge of a given cluster of RyRs, then successive activation of RyRs within the cluster would be markedly unidirectional and the shape of the spark would be skewed.

In addition to the model above, large Ca^{2+} sparks in embryonic myotubes compared to adult myotubes could be due to a combination of factors such as (1) an increased mean open time of the RyR channel; (2) an increased Ca^{2+} current through the RyR channel; (3) a limited Ca^{2+} removal capacity of the embryonic cell; (4) a larger number of RyRs open during the Ca^{2+} release event; and (5) the presence of an embryonic RyR-3 isoform. The first two factors are not directly tractable at the present time due to the absence of single-channel data in embryonic muscle. Also, the third factor may not be tractable; however, it is a likely contributor to a longer spark duration because the Ca^{2+} spark decay is controlled in part by the cell Ca^{2+} removal systems (Gomez et al., 1996; Santana et al., 1997; Lukyanenko et al., 1998). The last two factors deserve special consideration given the anatomical features of the embryonic myotube and the changes in RyR expression during development. In the late embryonic stages of development (E17 to birth at E19.5), the transverse (T) tubule/SR junctions are not properly formed. At these stages, the SR forms a wide mesh with multiple random contacts with longitudinally oriented T-tubules. Occasional double T-tubules forming pentadic junctions with the SR have been described (Franzini-Armstrong et al., 1991). These features suggest that the disposition and density and, presumably, the size and functional state of the T-tubule/junctional SR contacts are highly heterogeneous in the developing myotube. Large sparks may originate from embryonic cells both because junctional domains could be intrinsically larger at this stage and because active domains may recruit additional domains to produce Ca^{2+} release in larger areas of the cell. Furthermore, the loss of interactions between whole DHPRs and RyRs may lead to secondary losses in junctional components that could alter the microscopic architecture surrounding the RyRs in unforeseen ways. This could cause alterations in RyR density and activity which, when compounded by the anatomical heterogeneity of the embryonic myotube, may explain some of the results of the present study. This unsavory possibility deserves to be investigated. The presence of an embryonic RyR isoform (RyR-3) may also be a significant factor determining the behavior of sparks. RyR-3 is widely distributed in mouse skeletal muscle during the late embryonic and postnatal phase of muscle development and in adult muscle is restricted to the dia-

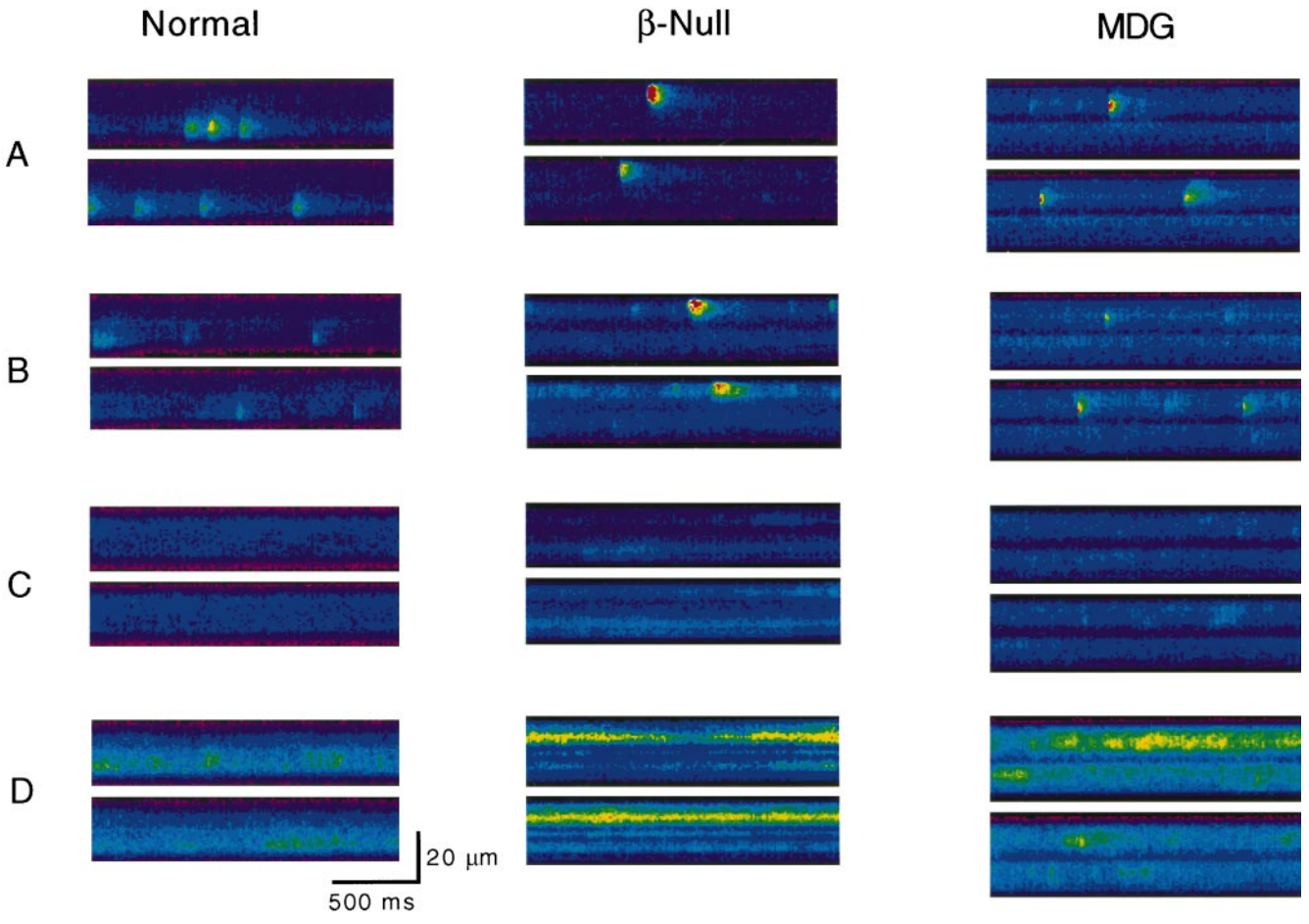

FIGURE 10 Inhibition of Ca^{2+} sparks by tetracaine. Line-scan images have a dimension of 15 μm (vertical) and 2.05 s (horizontal). Panel *A* shows two line scans from each cell during a control period. Panels *B* and *C* are line scans at the same cell location 10 and 30 min after addition of tetracaine at a final concentration of 0.2 mM to the bath solution. Panel *D* shows line scans at the same cell location after addition of caffeine at a final concentration of 0.1 mM.

phragm and soleus muscles (Bertocchini et al., 1997). The properties of RyR-3 channels suggest that this isoform may contribute to amplification of EC coupling initiated by RyR-1 (Sonnleitner et al., 1998) and could thus influence the properties of sparks from intercostal embryonic muscle. One would expect for example that a channel that amplifies EC coupling may also prolong spark duration, a hypothesis that we have begun to consider (Conklin et al., 1998b).

Assuming possibilities (1) through (5) do not change in β-null and *mdg* myotubes, specific arrangements of DHPRs and RyRs could potentially explain the differences in behavior of Ca^{2+} sparks in these mutant cells. In adult skeletal muscle, it was suggested that one half of RyR channels are controlled by DHPRs and therefore may be activated by voltage. The other half of RyR channels may be activated by Ca^{2+} released by the voltage-activated RyRs (Block et al., 1988; Shirokova et al., 1996). In β-null myotubes, RyRs are clustered and present at a density comparable to that of normal cells whereas DHPRs are present at a density lower than normal (Gregg et al., 1996; Strube et al., 1998). The excess of RyRs not controlled by voltage may increase the pool of RyR channels activated by Ca^{2+} in these cells. As a result, the density of Ca^{2+}-activated RyR channels may be much higher in the β-null cell than in the normal cell. One would expect that in these conditions, RyR channels would be more prone to near-neighbor activation by Ca^{2+}. A higher amplification of Ca^{2+} release during a spark due to a higher density of Ca^{2+}-activated RyR channels in junctional domains could explain the fact that sparks in β-null cells are larger in spatial and temporal dimension than sparks of normal cells.

The argument above implies that Ca^{2+} sparks in *mdg* cells should be even larger than those of β-null cells because all RyRs of *mdg* cells are Ca^{2+}-activated due to the absence of functional voltage sensors. Whereas some Ca^{2+} sparks in *mdg* myotubes were comparable to sparks in β-null cells, on the average this was not the case (Fig. 6). A mechanism by which RyR channels of *mdg* cells may be prevented from becoming activated during a spark could involve a negative feedback from the DHPR β_1 subunit which is known to be present in *mdg* cells (Gregg et al., 1996). This putative interaction between the DHPR β_1 subunit and the RyR-1 could terminate Ca^{2+} release during a spark and thus limit the spatial Ca^{2+} propagation. How-

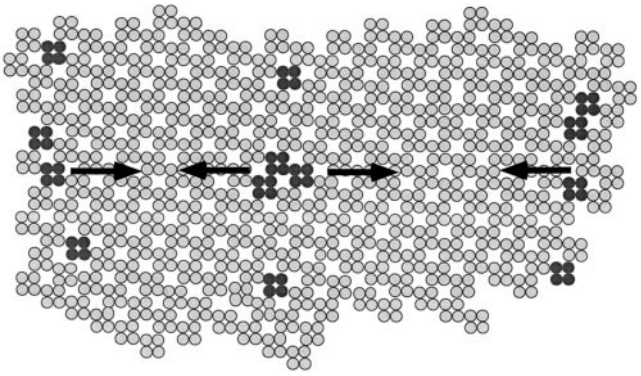

FIGURE 11 Model of large Ca^{2+} spark formation in embryonic muscle. The diagram shows a large cluster of RyRs arranged in a conventional side-to-side disposition described from myotubes in culture (Takekura et al., 1994). According to the tetrad size (26 nm on its side), the cluster is $\sim 0.6 \times \sim 0.3$ μm. RyR antibody staining features of this size and larger are typical of normal and mutant myotubes (Gregg et al., 1996). Initial activation of a few RyRs (shaded tetrads) leads to successive activation of other Ca^{2+}-sensitive RyRs in the cluster. Arrows indicate net direction of spread of activation depending on whether the spark is triggered near the center or near the edges of the cluster. If RyRs near the center lead the activation, the spark is nearly symmetrical. If RyRs near the edge lead the activation, the spark is skewed.

ever, it is unclear how Ca^{2+}-activated RyRs, if this is the ultimate explanation, can lead to an increase in Ca^{2+} spark duration in β-null cells and to the opposite effect in *mdg* cells. In summary, the present results raise the possibility that an interaction between the DHPR and the RyR may be constitutively present and removal of specific DHPR subunits would lead to alterations of the characteristics of the Ca^{2+} sparks. The potential effects of DHPR β_1 and α_{1S} subunits on the RyR channel are not expected to be mutually exclusive because in the normal cell both subunits are present in the complex at a 1:1 ratio. The proposed interactions could be further investigated in double mutant α_{1S}-null/β-null embryos and in cDNA-transfected myotubes in culture.

Supported by National Institutes of Health grant HL-47053 (R.C., P.A.P., and R.G.G.) and an American Heart Association Wisconsin Affiliate Predoctoral Fellowship (M.C.).

REFERENCES

Adams, B. A., T. Tanabe, A. Mikami, S. Numa, and K. G. Beam. 1990. Intramembrane charge movement restored in dysgenic skeletal muscle by injection of dihydropyridine receptor cDNAs. *Nature.* 346:569–572.

Bertocchini, F., C. E. Ovitt, A. Conti, V. Barone, H. R. Scholer, R. Bottinelli, C. Reggiani, and V. Sorrentino. 1997. Requirement for the ryanodine receptor type 3 for efficient contraction in neonatal skeletal muscles. *EMBO J.* 16:6956–6963.

Beurg, M., M. Sukhareva, C. Strube, P. A. Powers, R. Gregg, and R. Coronado. 1997. Recovery of Ca^{2+} current, charge movements, and Ca^{2+} transients in myotubes deficient in dihydropyridine receptor β_1 subunit transfected with β_1 cDNA. *Biophys. J.* 73:807–818.

Blatter, L. A., J. Huser, and E. Rios. 1997. Sarcoplsmic reticulum Ca^{2+} release flux underlying Ca^{2+} sparks in cardiac muscle. *Proc. Natl. Acad. Sci. USA.* 94:4176–4181.

Block, B., A., T. Imagawa, K. P. Campbell, and C. A. Franzini-Armstrong. 1988. Structural evidence for direct interaction between the molecular components of the transverse tubule/sarcoplasmic reticulum junction in skeletal muscle. *J. Cell Biol.* 107:2587–2600.

Carl S. L., K. Felix, A. H. Caswell, N. R. Brandt, W. J. Ball, Jr., P. L. Vaghy, G. Meissner, and D. G. Ferguson. 1995. Immunolocalization of sarcolemmal dihydropyridine receptor, and sarcoplasmic reticular triadin, and ryanodine receptor in rabbit ventricle, and atrium. *J. Cell Biol.* 129:673–682.

Cannell, M. B., H. Cheng, and W. J. Lederer. 1995. The control of calcium release in heart muscle. *Science.* 268:1045–1049.

Cheng, H., W. J. Lederer, and M. B. Cannell. 1993. Calcium sparks: elementary events underlying excitation-contraction coupling in heart muscle. *Science.* 262:740–744.

Conklin, M., P. Powers, R. Gregg, and R. Coronado. 1997. Spontaneous calcium sparks in dihydropyridine receptor β_1 knock-out skeletal muscle. *Biophys. J.* 72:A45.

Conklin, M., P. Powers, R. Gregg, and R. Coronado. 1998a. Molecular determinants of calcium sparks in skeletal muscle. *Biophys. J.* 74:A235.

Conklin, M., C. Strube, V. Sorrentino, and R. Coronado. 1998b. Contribution of ryanodine receptor type 3 to Ca^{2+} sparks in embryonic skeletal muscle. Biophysical Society Meeting Baltimore, MD, February 13–17, 1999. Submitted abstract.

Franzini-Armstrong, C. 1991. Simultaneous maturation of transverse tubules and sarcoplasmic reticulum during muscle differentiation in the mouse. *Dev. Biol.* 146:353–363.

Garcia-Martinez, J., T. Tanabe, and K. G. Beam. 1994. Relationship of calcium transients to calcium currents and charge movements in myotubes expressing skeletal and cardiac dihydropyridine receptors. *J. Gen. Physiol.* 103:125–147.

Gregg, R. G., A. Messing, C. Strube, M. Beurg, R. Moss, M. Behan, M. Sukhareva, S. Haynes, J. A. Powell, R. Coronado, and P. A. Powers. 1996. Absence of the beta subunit (*cchbl*) of the skeletal muscle dihydropyridine receptor alters expression of the alpha(1) subunit and eliminates excitation-contractioncoupling. *Proc. Natl. Acad. Sci. USA.* 93: 13961–13966.

Gomez, A. M., H. Cheng, W.J. Lederer, and D. M. Bers. 1996. Ca^{2+} diffusion and sarcoplasmic reticulum transport both contribute to Ca^{2+} decrine during Ca^{2+} sparks in rat ventricular myocytes. *J. Physiol.* 496.2:575–581.

Klein, M. G., H. Cheng, L. F. Santana, Y.-H. Jiang, W. J. Lederer, and M. F. Schneider. 1996. Two mechanisms of quantized calciun release in skeletal muscle. *Nature.* 379:455–458.

Lacampagne, A., W. J. Lederer, M. F. Schneider, and M. G. Klein. 1996. Repriming and activation alter the frequency of stereotyped discrete Ca^{2+} release events in frog skeletal muscle. *J. Physiol.* 497.3:508–588.

Lukyanenko, V., T. Weisner, and S. Gyorke. 1998. Termination of Ca^{2+} release during Ca^{2+} sparks in rat ventricular myocytes. *J. Physiol.* 507.3:667–677.

Nakai, J., R. T. Dirksen, H. T. Nguyen, I. N. Pessah, K. G. Beam, and P. D. Allen. 1996. Enhanced dihydropyridine receptor activity in the presence of ryanodine receptor. *Nature.* 380:72–75.

Parker, I., W.-J. Zang, and W. G.Wier. 1996. Ca^{2+} sparls involving multiple Ca^{2+} release sites along Z-lines in rat heart cells. *J. Physiol.* 497.1:31–38.

Protasi, F., X.-H. Sun, and C. Franzini-Armstrong. 1996. Formation and maturation of the calcium channel release apparatus in developing and adult avian myocardium. *Dev. Biol.* 173:265–278.

Rios, E., J. Ma, and A. Gonzalez. 1991. The mechanical hypothesis of excitation-contraction coupling in skeletal muscle. *J. Muscle Res. Cell Mot.* 12:127–135.

Santana, L. F., H. Cheng, A. M. Gomez, M. B. Cannell, and W. J. Lederer. 1996. Relation between the sarcolemmal Ca^{2+} current and Ca^{2+} sparks and local control theories for cardiac excitation-contraction coupling. *Circ. Res.* 78:166–171.

Santana, L. F., E. G. Kranias, and W. J. Lederer. 1997. Calcium sparks and excitation-contraction coupling in phospholamban-deficient mouse ventricular myocytes. *J. Physiol.* 503.1:21–29.

Shacklock P. S., W. G. Wier, and C. W. Balke. 1996. Local calcium transients (Ca^{2+} sparks) originate at transverse tubules in rat heart cells. *J. Physiol.* 487:601–608.

Shirokova, N., J. Garcia, G. Pizarro, and E. Rios. 1996. Ca^{2+} release from the sarcoplasmic reticulum compared in amphibian and mammalian skeletal muscle. *J. Gen. Physiol.* 107:1–18.

Shirokova, N., and E. Rios. 1997. Small event Ca^{2+} release: a propable precursor of Ca^{2+} sparks in frog skeletal muscle. *J. Physiol.* 502.1:3–11.

Sonnleitner, A., A. Conti, F. Bertocchini, H. Schindler, and V. Sorrentino. 1998. Functional properties of the ryanodine receptor type 3 (RyR3) Ca^{2+} release channel. *EMBO J.* 17:2790–2798.

Strube, C., M. Beurg, P. A. Powers, R. G. Gregg, and R. Coronado. 1996. Reduced Ca^{2+} current, charge movement, and absence of Ca^{2+} transients in skeletal muscle deficient in dihydropyridine receptor beta-1 subunit. *Biophys. J.* 71:2531–2543.

Strube, C., M. Sukhareva, P. A. Powers, R. G. Gregg, and R. Coronado. 1998. Molecular origin of the L-type Ca^{2+} current of skeletal muscle myotubes selectively deficient in dihydropyridine receptor beta-1a subunit. *Biophys. J.* 75:207–217.

Takekura, H., L. Bennett, T. Tanabe, K. G. Beam, and C. Franzini-Armstrong. 1994. Restoration of junctional tetrads in dysgenic myotubes by dihydropyridine receptor cDNA. *Biophys. J.* 67:793–803.

Tanabe, T., K. G. Beam, B. A. Adams, T. Niidome, and S. Numa. 1990. Regions of skeletal muscle dihydropiridine receptor critical for excitation-contraction coupling. *Nature.* 346:567–569.

Tsugorka, A., E. Rios, and L. A. Blatter. 1995. Imaging elementary events of calcium release in skeletal muscle cells. *Science.* 269:1723–1726.